Geophysical Journal International

Geophys. J. Int. (2015) **202,** 77–93
GJI Seismology

doi: 10.1093/gji/ggv235

Extended fault inversion with random slipmaps: a resolution test for the 2012 M_w 7.6 Nicoya, Costa Rica earthquake

José Ángel López-Comino,[1,2] Daniel Stich,[1,2] Ana M.G. Ferreira[3,4] and Jose Morales[1,2]

[1]*Instituto Andaluz de Geofísica, Universidad de Granada, E-18071 Granada, Spain. E-mail: jalopezcomino@ugr.es*
[2]*Departamento de Física Teórica y del Cosmos, Universidad de Granada, E-18071 Granada, Spain*
[3]*Department of Earth Sciences, Faculty of Maths & Physical Sciences, University College London, WC1E6BT, United Kingdom*
[4]*CEris, ICIST, Instituto Superior Tecnico, Universidade de Lisboa, P-1049-001 Lisboa, Portugal*

Accepted 2015 June 1. Received 2015 May 25; in original form 2014 December 4

SUMMARY

Inversions for the full slip distribution of earthquakes provide detailed models of earthquake sources, but stability and non-uniqueness of the inversions is a major concern. The problem is underdetermined in any realistic setting, and significantly different slip distributions may translate to fairly similar seismograms. In such circumstances, inverting for a single best model may become overly dependent on the details of the procedure. Instead, we propose to perform extended fault inversion trough falsification. We generate a representative set of heterogeneous slipmaps, compute their forward predictions, and falsify inappropriate trial models that do not reproduce the data within a reasonable level of mismodelling. The remainder of surviving trial models forms our set of coequal solutions. The solution set may contain only members with similar slip distributions, or else uncover some fundamental ambiguity such as, for example, different patterns of main slip patches. For a feasibility study, we use teleseismic body wave recordings from the 2012 September 5 Nicoya, Costa Rica earthquake, although the inversion strategy can be applied to any type of seismic, geodetic or tsunami data for which we can handle the forward problem. We generate 10 000 pseudo-random, heterogeneous slip distributions assuming a von Karman autocorrelation function, keeping the rake angle, rupture velocity and slip velocity function fixed. The slip distribution of the 2012 Nicoya earthquake turns out to be relatively well constrained from 50 teleseismic waveforms. Two hundred fifty-two slip models with normalized L1-fit within 5 per cent from the global minimum from our solution set. They consistently show a single dominant slip patch around the hypocentre. Uncertainties are related to the details of the slip maximum, including the amount of peak slip (2–3.5 m), as well as the characteristics of peripheral slip below 1 m. Synthetic tests suggest that slip patterns such as Nicoya may be a fortunate case, while it may be more difficult to unambiguously reconstruct more distributed slip from teleseismic data.

Key words: Inverse theory; Controlled source seismology; Earthquake source observations; Theoretical seismology.

INTRODUCTION

The propagation of earthquake rupture leaves a signature in elastic waves and static displacement fields observed at the Earth's surface. In consequence, from appropriate seismic or geodetic observations we may try to estimate properties of the seismic source such as duration and extent of the rupture, the velocity of rupture propagation, and possibly the asymmetry or other non-uniformities of the rupture. The most complete interpretation of finite fault effects is provided by full kinematic slip inversion, aiming at resolving the spatiotemporal distribution of slip along the fault. Extended, or finite fault slip inversion is typically based on the representation of the seismic wavefield from a surface integral over the fault, evaluating the product of the areal moment tensor density and the local spatial derivatives of the Green's function tensor (Aki & Richards 2002). Most commonly, a plane, rectangular fault model is discretized into a regular array of point sources or subfaults, and the inversion process in its general form consists in determining the slip history at each subsource (e.g. Festa & Zollo 2012). Results from full slip inversion are useful for many aspects of seismology from characterizing active faults to simulating (strong) ground motion, but most importantly, they also provide invaluable information about what typically happens during the earthquake source process.

Given the relevance of slip models, a major concern within the community is the resolution and stability of the inversions. There are numerous examples in the seismological literature where different

inversion strategies, different assumptions and different parameter choices sets have led to significantly different and sometimes contradictory models for the same earthquake (see e.g. Weston *et al.* 2012 for a review). Ambiguity in extended fault inversion has been documented since the early applications to recordings from the 1979 Imperial Valley, California earthquake (Olson & Apsel 1982; Hartzell & Heaton 1983; Archuleta 1984). These studies show that quite different slip histories could fit the waveform data satisfactorily, and establish the need to use stabilizing constraints such as smoothness, minimum moment and positivity of the solution. Another already classic example for uncertainties in extended fault inversion is the 1999 Izmit earthquake (Turkey), for which strikingly different slip distributions have been proposed by different groups (Yagi & Kikuchi 2000; Bouchon *et al.* 2002; Delouis *et al.* 2002; Sekiguchi & Iwata 2002). In the case of the Izmit earthquake, the available data are probably insufficient to constrain the rupture process (Beresnev 2003; Ide *et al.* 2005). But even exceptionally well-recorded events such as the 2004 Parkfield earthquake show remarkable variability in rupture models obtained from different data subsets or different parameterizations (e.g. Custodio *et al.* 2005; Hartzell *et al.* 2007).

Such examples highlight the non-uniqueness of the inversion, which may be aggravated by the incomplete and relatively sparse sampling of the wavefield at the earth surface, noise and other measurement errors, and our incomplete knowledge of earth's internal structure, linking to imperfect Green's functions (e.g. Cohee & Beroza 1994; Sekiguchi *et al.* 2000; Graves & Wald 2001; Ferreira *et al.* 2011). The challenge is that information on the spatial heterogeneity of slip and rupture propagation comes packaged in rather subtle features of the waveforms. Discrepancies between the data and the forward model predictions should be small in order to support that we used adequate data and forward modelling. On the other hand, appropriate fits alone do not guarantee that the inverted slip model is a useful approximation to the actual rupture pattern. A first important coordinated effort to understand the limitations in extended slip inversion has been the SPICE blind test, where different approaches have been applied in a controlled environment, with overall discouraging initial results with respect to their capability to recover the target slip distribution (Mai *et al.* 2007; Shao & Ji 2012). Ongoing efforts in earthquake source model validation such as the source inversion validation (SIV) project, http://equake-rc.info/sivdb/wiki/ are continuing to actively address these issues.

From the above, it is clear that great care with uncertainties needs to be taken when performing extended fault source inversions, up to the point that we should probably depart from the traditional view of optimization approaches as tools to produce one single best model (Tarantola & Valette 1982; Tarantola 2006). Basically, the key question with any slip model is whether a substantially different slipmap, or several of them, would explain the recorded data as well. This consciousness has led to numerous recent attempts to estimate uncertainties. Several authors have conducted multiple fault inversions for different parameter settings and data selections, presenting multiple source models, or the mean and standard deviation from an ensemble of possible models (e.g. Custodio *et al.* 2005; Stich *et al.* 2005; Liu *et al.* 2006; Hartzell *et al.* 2007; Gallovič & Zahradník 2012). On the other hand, in nonlinear search schemes, a large number of potential slip models are tested during the random walk, so they are intrinsically well suited for exploring uncertainties (e.g. Peyrat & Olsen 2004; Piatanesi & Lorito 2007; Piatanesi *et al.* 2007). Finally, the ensembles of models from a global search can be corrected for the irregular sampling of the model space, leading to formal uncertainties from a Bayesian appraisal of the problem, where the likelihood for the different model parameters is quantified in an *a posterior* probability density function (e.g. Fukuda & Johnson 2008; Monelli & Mai 2008; Fichtner & Tkalcic 2010; Minson *et al.* 2013). Fully nonlinear Bayesian approaches can also show whether the available data can constrain the rupture process, leading to narrow marginal probability density functions for appropriate data (Minson *et al.* 2014).

EXTENDED SOURCE INVERSION THROUGH FALSIFICATION

Since the non-uniqueness of source inversion tends to manifest in the existence of different slip models with comparable level of fit, low misfit for any given model is of limited significance. The more significant observation is the failure of a given source model to fit the observations within a typical and acceptable level of mismodelling, meaning that this particular model has to be wrong. This asymmetry lends itself to a treatment of the extended source inverse problem from a Popperian viewpoint of scientific logic (Popper 1934; Tarantola 2006): A tested slip model cannot be considered verified because of its good performance, but it can be considered falsified if it performs badly. In the latter case, the falsified source model can be cancelled from the ensemble of possible models. Here we apply an Popperian inversion strategy that involves the generation of a representative set of slip distributions, comparison of the corresponding forward predictions to the recorded data, and the generation of the solution to the inverse problem as an assembly of all those trial models that have not been falsified on account of unacceptable fits. This approach is different from Bayesian approaches as it replaces the gradual evaluation of model performance in terms of probabilities by logic falsification of inappropriate rupture models, and uses the ensemble of all possible slip models instead of the posterior probability density function of the model parameters. We introduce our approach as an alternative to Bayesian inversions since it can be kept simpler due to its non-positivistic focus and it avoids the intrinsic difficulties with interpreting complex probability distributions in many dimensions (Tarantola 2006).

Working with the ensemble of possible source models provides more direct access to ambiguities and uncertainties of the inversion, compared to probability solutions where the display of uncertainties becomes a problem. In particular, the most accessible representation through marginal probability densities provides single parameter errors, which means they include the interactions with other model parameters only implicitly. In reality, in extended source models there must be strong trade-offs among the subfault parameters in order to produce similar waveforms by summing up their individual contributions. Errors of individual parameter may provide a good representation of uncertainties if all members of the solution ensemble are similar, like showing the same number of principal slip patches in similar positions. In such well-constrained cases, marginal probability functions are narrow, and an average solution is close to all individual solutions (e.g. Liu *et al.* 2006; Minson *et al.* 2014). Otherwise, if the solution ensemble reveals fundamental ambiguities of the inversion, using the mean or maximum likelihood solution may blend significantly different slip patterns into a single, overly smoothed model. This model may show fairly low similarity to all individual models of the solution ensemble and may not even produce an appropriate fit to the data, yet the user often accepts it as the best model. The marginal probability distributions become broad, hiding the trade-offs among parameters. In

fact, they are reintroducing spurious models that have obtained a low score previously, thus being inefficient in the sense of Popperian falsification.

Also in Popperian inversion, the ensemble of models may become too large or heterogeneous for direct interpretation, and any contraction of the solution ensemble into an average model and individual parameter errors may be prone to similar problems of oversimplification. However, full slip ensembles allow for a two-step assessment of the results, consisting of some pattern recognition and classification into subsets of solutions with similar characteristics, followed by the application of simplified statistics to each subset. The intention of our inversion approach is to keep the model space small in order to keep the solution ensemble as manageable as possible. We show that assuming a realistic, empirical autocorrelation function for the heterogeneity of fault slip (Mai & Beroza 2002) there exist only a few thousand different slip distributions that we might optimistically hope to distinguish. Hence, a relatively coarse sampling of the space of conceivable rupture models is sufficient for Popperian inversion, where we are not as much interested in the fine tuning of the optimal solution, but rather in establishing uncertainties, which will be achieved by falsifying a—hopefully large—percentage of the trial models. The focus on falsification does not require a guided search that would concentrate new trial models in previously identified areas of low misfit. Finally, at this stage, we will keep the rake angle, the rupture velocity, as well as the slip velocity function on all subfaults fixed. We readdress these restrictive assumptions in the discussion section.

This strategy for extended source inversion can be applied to any observation for which we can solve the forward problem, in particular seismic, geodetic or tsunami data at suitable recording distances, or any combination of them. Here we illustrate the scheme through extended fault inversion from seismic body waves recorded at teleseismic distances between 30° and 95°. This has become a routine set-up in teleseismic slip inversion, because of the general availability of appropriate recordings for all major earthquakes worldwide, the comparably unproblematic nature of the forward problem, as well as the availability of suitable and well-tested codes (e.g. Kikuchi & Kanamori 1982, 1991, 2003; Ji *et al.* 2002). Front-end problems of the inversion such as data coverage and quality, pre-processing and assumptions on Earth structure are typically minor for body-wave teleseismic data for the distances considered (e.g. Weston *et al.* 2014), however the intrinsic non-uniqueness of the inversion persists. We first generate slipmaps and synthetic forward predictions for a teleseismic recording geometry to illustrate the asymmetry between data similarity and model similarity. Next we perform the complete inversion procedure, comparing synthetic data to observations and analysing the set of solutions. We select for these exercises the 2012 September 5, M_w 7.6 earthquake beneath the Nicoya Peninsula, Costa Rica earthquake as an example of a recent earthquake with relatively large moment magnitude and presumably simple slip distribution (Hayes 2012; Ye *et al.* 2013; Yue *et al.* 2013).

A MODEL SPACE OF PSEUDO-RANDOM SLIPMAPS

The first step of the inversion scheme is the generation of a representative set of slip models that can be evaluated according to their ability or inability to explain the recorded data. For fixed rupture velocity, rake and slip velocity function, the model variability consists in different distributions of fault slip. We discretize a plane fault into a regular mesh of subfaults with constant slip, resulting typically in a few hundred of model parameters to be determined, depending on the size of the fault and the subfaults. Such a model space is too large for a full exploration through systematic grid search, varying all subfault displacements independently with some appropriate increment for relative slip. Fortunately, according to empirical experience, inverted earthquake slip maps are not random fields pixel by pixel. They show a characteristic partitioning of short and long wavenumber components, resulting in the familiar pattern of one or more distinct slip patches. This observation allows for using stochastic modelling to generate slip maps reminiscent of those obtained from inversion (Mai & Beroza 2002; Lavallée & Archuleta 2003; Lavallée *et al.* 2006). Among several tested autocorrelation functions, a von Karman distribution provides the best fit to power spectral densities of inverted fault slip distributions (Mai & Beroza 2002). However, the differences between von Karman, exponential and fractal fits are relatively small due to the limited range of spatial wavenumbers in data derived models, subject to fault discretization and smoothing. Independent support comes from borehole logs, where the power spectra of parameter variations over a larger range of wavenumbers can also be adjusted by von Karman distributions (Hollinger 1996; Dolan *et al.* 1998; Bean *et al.* 1999). It appears plausible that heterogeneity in the crust and heterogeneity of fault slip may have similar statistical properties.

We use a von Karman autocorrelation function to produce pseudo-random slip distributions following the procedure in Mai & Beroza (2002). The correlation function prescribes the amplitude spectra of slip, while the phase is generated randomly, and the two-dimensional slip distribution is computed through spectral synthesis (Pardo-Igúzquiza & Chica-Olmo 1993). We assume a correlation length along strike of 1/3 of the fault length plus two subfaults, and 1/3 of the fault width plus one subfault in downdip direction, according to the scaling laws obtained by Mai & Beroza (2002). We choose a Hurst exponent of $H = 1$, translating to an expected fractal dimension of two for our model scenario of a plane rupture surface, known rupture velocity and known slip velocity function. Among the generated 2-D fields, we keep only those with slip concentrated in the centre, that is, average slip in the inner 50 per cent of the fault model area should be at least 0.4 times the variance. This threshold penalizes random fields with large amplitudes at the borders, which are not desired for earthquake slip distributions where the displacement should tend to zero at the limit of the rupture area. If the fault model reaches the free surface, the inner area for slip validation is extended to the upper model boundary. At this point, the random 2-D fields still have a mean value of zero as obtained from the pseudo-random distributions, and need to be shifted in amplitude to obtain realistic earthquake slip distributions with net seismic moment different from zero. For this purpose, a constant of 0.5 times the variance is added to the slip amplitudes, and the remaining negative values are truncated to zero. In this way we enforce a positivity constraint on slip and implement the perimeter of the earthquake where rupture has come to an end. Examples of different slip distributions obtained by this procedure are shown in Fig. 1.

An important aspect for the viability of the inversion is the number of required trial models. Possibly a few slip models may be sufficient to show that a given inversion problem is ambiguous, but a large number of models should be tested in order to support that a slip model is reasonably well resolved. The problem is manageable thanks to the linearity of the forward problem, meaning that similar models will generate similar data; hence we do not

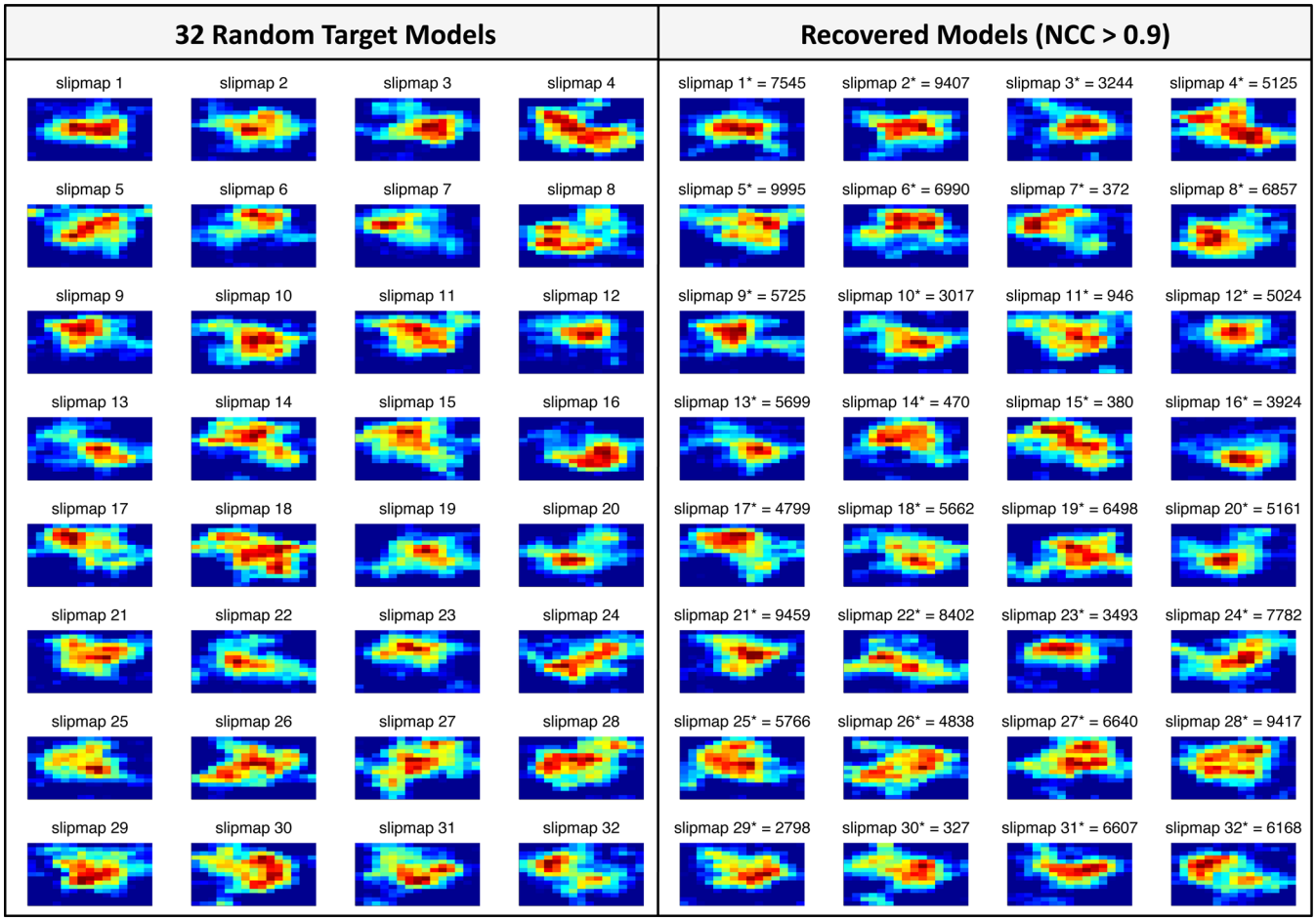

Figure 1. Samples from the inventory of 10 000 synthetic slip distributions generated for von Karman power spectral density with fractal dimension of two, pseudo-random phase values, and appropriate post-processing in order to emulate earthquake slip patterns reminiscent of real data inversion results. The left part of the figure shows the first 32 random models obtained for a single seed, and the right part shows the most similar counterparts among the remaining models (the labels indicate the reference slipmap with a star, and the number of the random simulation corresponding to the most similar slipmap). Similarity is quantified in terms of Normalized zero-lag Cross Correlation (NCC). The figure illustrates the diversity of slipmaps and the repeated occurrence of similar slipmaps among the inventory, suggesting that we obtained a suitable representation of the model space. Slipmap amplitudes are not to scale.

expect that models with minor differences could be distinguished from observations. In Popperian inversion, we are interested in evaluating different models rather than similar models. Above or below the chosen threshold for falsification there is no sensitivity to the different performance of marginally different models, because the model evaluation is a yes–no question. This justifies keeping the sampling of the model space relatively coarse, however we are still interested in a model inventory that incorporates all fundamentally different rupture patterns. Random model generation cannot guarantee completeness in this sense, because it is intrinsically unknown in which one of the simulations a specific rupture pattern will be generated. A pragmatic answer can be given through a control sample. If we consider that slip models showing a normalized zero-lag cross correlation larger than 0.9 are definitely similar regarding the distribution of slip, we generally find such a high-similarity for slipmaps chosen at random among an inventory of 10 000 models (Fig. 1). The number of 10 000 slip models is still a rather cautious choice, and we could further reduce the model space by eliminating redundant slipmaps. For the purpose of this study, we decide to keep all 10 000 models, because in our set-up this amount is unproblematic considering computational efficiency.

SYSTEMATIC FORWARD MODELLING FOR THE 2012 NICOYA EARTHQUAKE

In order to evaluate the generated slip models in terms of their ability to explain recorded data, we have to solve the forward problem and apply some appropriate similarity or distance measure for the comparison between synthetic predictions and observations. Both aspects will be exemplified with the case of the 2012 September 5 Nicoya earthquake. The earthquake occurred beneath the Nicoya Peninsula on the Pacific coast of Costa Rica and can be attributed to the subduction of the Cocos Plate below the Caribbean Plate. It has been characterised as a nearly pure reverse faulting earthquake with NW–SE strike, parallel to the plate boundary, and moment magnitude of 7.6 (global CMT catalogue, Dziewonski *et al.* 1981; Ekström *et al.* 2012), making it the largest Central American event since the destructive January 2001 El Salvador earthquake. Four studies have proposed finite source models for the Nicoya earthquake so far (Hayes 2012; Ye *et al.* 2013; Yue *et al.* 2013; Protti *et al.* 2014). The first two studies use teleseismic data and two different inversion schemes (Ji *et al.* 2002; Kikuchi & Kanamori 2003, respectively), Protti *et al.* (2014) use geodetic data, and Yue *et al.* (2013) combines teleseismic data with local seismic and geodetic observations. There is reasonable agreement among the

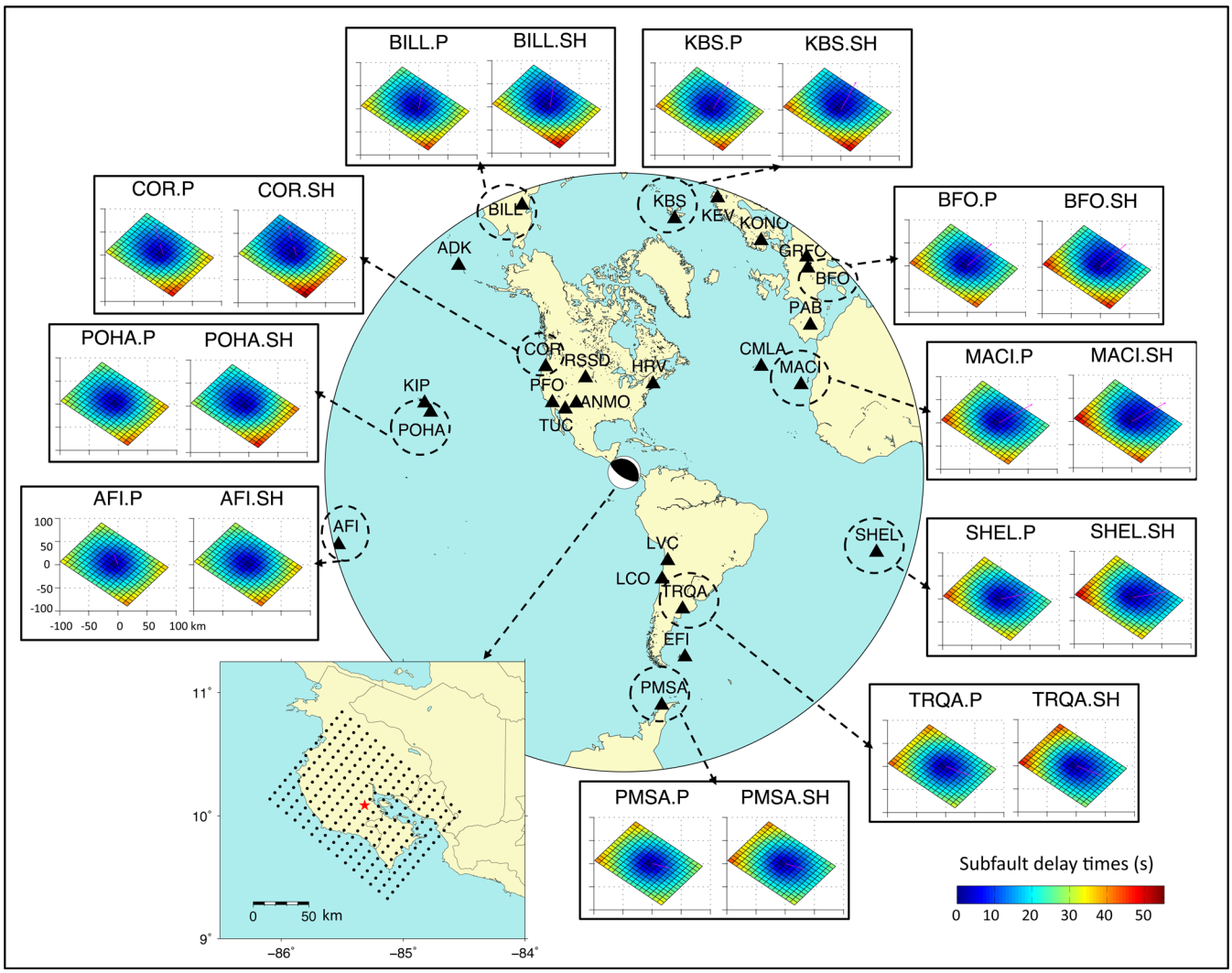

Figure 2. Distribution of 25 teleseismic broadband stations (triangles) selected for body wave inversion of the 2012 Nicoya earthquake (red star). On the lower left, we show the subsource parameterization of the fault plane, coincident with the shallow, NE-dipping subduction interface. Numerical values of parameters are given in the text. Surrounding the station map, we present examples for the distribution of subfault delay times for *P* and *S* waves at selected stations.

studies, suggesting that slip is concentrated in one single patch, about 70 km by 50 km in size. Peak slip amplitudes are ∼3 m, and slightly larger (∼4 m) in the purely geodetic inversion. The proposed velocity of rupture propagation is 2.5–3.0 km s^{-1}. There are discrepancies considering hypocentral depth, ranging from 40 km (Hayes 2012) to 13 km (Yue *et al.* 2013), with an associated shift of the hypocentre closer to the Middle American Trench. However, the main slip patch from extended fault inversion is close to 30 km depth in all cases. This is consistent with the centroid depth of 29.7 km reported in the global CMT catalogue. Accordingly, the Nicoya earthquake seems to combine a relatively large moment magnitude and rupture area with a presumably simple slip distribution, offering a useful example to explain and apply our inversion scheme.

We translate slipmaps into predictions for vertical *P* waves and horizontal *S* waves at the locations of 25 seismic broad-band stations at teleseismic distances from Costa Rica (Fig. 2). The selected stations belong to the Global Seismographic Network operated by IRIS and USGS, and were chosen according to azimuthal coverage and data quality for the Nicoya recordings. As for many other circum-Pacific earthquakes, the ocean–continent distribution influences the teleseismic coverage. We recall that the principles of the inversion scheme are independent of the forward modelling operator and type of data used, as well as that there are available GPS and strong motion data for the Nicoya earthquake (Yue *et al.* 2013; Protti *et al.* 2014) that might be useful to further restrict the solution set by falsifying additional slip models that cannot explain local data. Here, our priority is on understanding uncertainties of slip inversion rather than revising the source model of this particular earthquake, and we limit the inversion to this representative sample of teleseismic data for the sake of generality. We translate slip maps into a fault model assuming rupture across a plane surface with strike N310°E, dip 24° and rake 97° (Ye *et al.* 2013). For the size of the fault model, a choice that in principle has to be made according to waveform inspection or by educated guess, we build on previous work (Hayes 2012) and discretize the fault surface in 15 times 15 subfaults with dimensions of 10 km along strike and 8 km along dip (Fig. 2). Rupture starts at the centre of the fault model, associated with coordinates of 10.085° N, 85.315°W and depth of 35 km. We tested different rupture velocity by trial and error and choose 2.5 km s^{-1}, consistent with previous teleseismic inversions (Hayes 2012; Ye *et al.* 2013).

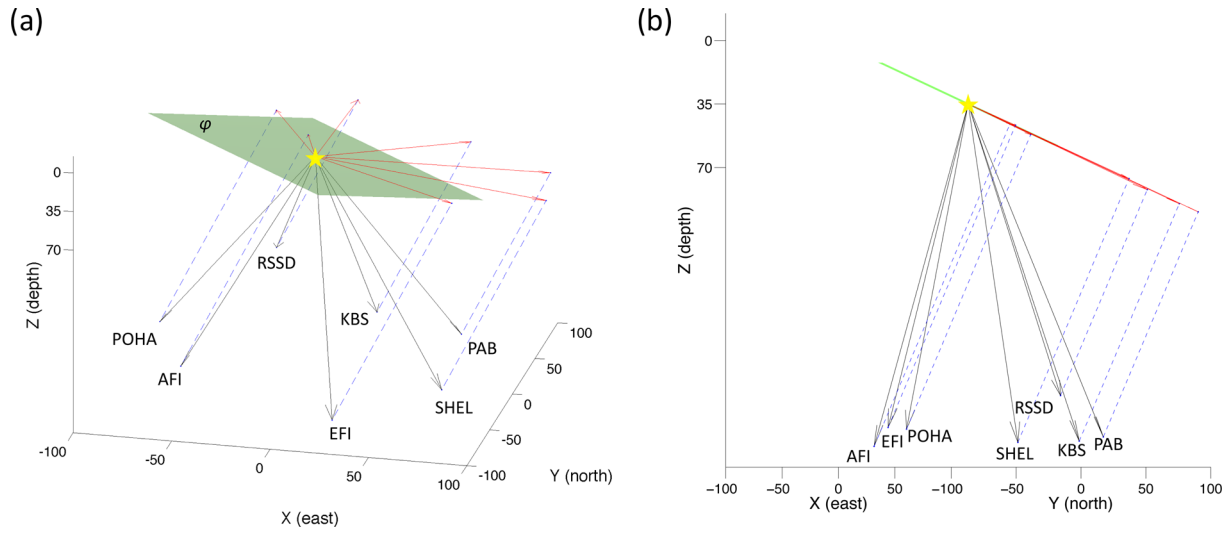

Figure 3. Geometry of fault plane (green plane, φ), downgoing seismic ray or take-off vector (black vectors, $\vec{r}$) and projection of the take-off vector on the fault plane (red vectors, $proj_{\varphi}\vec{r}$) for some seismic stations (see Fig. 2) for *P* waves. $\vec{r}$ is a unit vector and $\left|proj_{\varphi}\vec{r}\right|$ varies between 0 and 1. The perspective view (a) and the vertical cross section perpendicular to strike (b) are shown. Blue dotted lines show the paths followed for take-off vector projections on the fault plane. The hypocentre is identified with a yellow star and labels are in km.

The solution of the forward modelling problem involves the computation of the Green's functions for *P* and *S* waves for each pair of subfault and station, as well as the scaling, alignment and superposition of all subfault contributions. We use unfiltered displacement data in the inversions and compute Green functions using the Kikuchi and Kanamori inversion package, including a propagator matrix approach in a simplified Jeffreys and Bullen earth model (Kikuchi & Kanamori 2003). We assume a single triangle as slip velocity function for each subfault, and select a constant half duration of 3 s for this earthquake consistent with the subfault discretization and the frequency content of the target displacement waveforms. We assign delay times to each subfault Green functions taking into account the arrival time of the rupture front as well as the geometry of fault plane and downgoing seismic ray.

$$t_{rup,ij} = \frac{x_j}{v_r} - \frac{\left|proj_{\varphi}\vec{r}\right|_i x_j \cos\theta_{ij}}{c}. \quad (1)$$

The first term is equal to the length of the subfault position vector, x_j (from the hypocentre) divided by the rupture speed, v_r. The second term corresponds to the projection of the take-off vector, $\vec{r}$, onto the subfault position vector, divided by the local phase velocity, c. The term, $\left|proj_{\varphi}\vec{r}\right|_i$, varies between 0 and 1, depending on the position of the each seismic station, i, and the geometry of fault plane, φ (Fig. 3). The angle θ_{ij} is defined between the subfault position vector and the projection of the take-off vector for each seismic station. The projection and the generally larger velocity of wave propagation compared to rupture propagation makes the second term smaller than the first. Hence, the rupture term, with radial symmetry, dominates delay times (Fig. 2). Finally, the prediction for each slip distribution is obtained as a weighted sum of all subfault contributions over the fault plane. For this purpose, slip velocity functions for each subfault are scaled by the corresponding local displacement discontinuity. The area of the overall earthquake source time function is normalized to the net seismic moment of the earthquake (2.93×10^{20} Nm, Hayes 2012). The normalization implies that scalar seismic moment is not a parameter we address in inversion.

Before comparing the model predictions to recordings from the Nicoya earthquake, we use synthetic waveforms to illustrate the main potential of teleseismic body wave data to distinguish between different rupture patterns. High resolving power requires that notably different slip models translate to notably different seismograms, while our working hypothesis in this study is more pessimistic: The non-uniqueness of the inversion corresponds to the existence of notably different models with similar forward predictions. Fig. 4 displays forward modelling predictions for 32 slipmaps from Fig. 1 in waveform panels, illustrating how the variability of slipmaps translates into variability of predicted data. A wide range of different rupture patterns on a 150 km by 120 km fault model boils down to relatively minor differences in waveforms. This comparison is chilling, because the variability of waveforms is not substantially larger than the level of mismodelling that we may be forced to accept in some applications to real data. The general similarity of forward modelling predictions explains the familiar dependence of slip inversions on details of the procedure such as data selection, seismogram alignment, earth model selection and the choice of regularization parameters, misfit norm, elementary slip function or rupture speed, among others. Also changes in the synthetics for different focal mechanisms or hypocentral depths may become important, causing additional trade-offs with point source parameters, which are typically outsourced from extended fault inversion.

Finally, we use synthetic waveforms to analyse if the similarity in waveforms and the similarity in slipmaps, albeit different in size, may at least follow a monotonic relationship. That is, more different slipmaps would consistently correspond to more different seismograms. We can easily answer this question in the negative, analysing similarity among slip models and their corresponding predictions (Fig. 5). For the sake of simplicity, we quantify similarity using the normalized cross correlation coefficient for both, models and data. As suspected, slipmap correlations are smaller than seismogram correlations, even though subfault displacements are always positive numbers and, unlike seismogram amplitudes, can never interfere destructively. The scatter of points indicates that the relationship is not monotonic. The non-uniqueness of the problem becomes particularly well illustrated through pairs of models with low similarity (cross correlation <0.45) that translate into sets of seismograms with average cross correlations larger than 0.9 (red box in Fig. 5). These cases mostly correspond to pairs of models

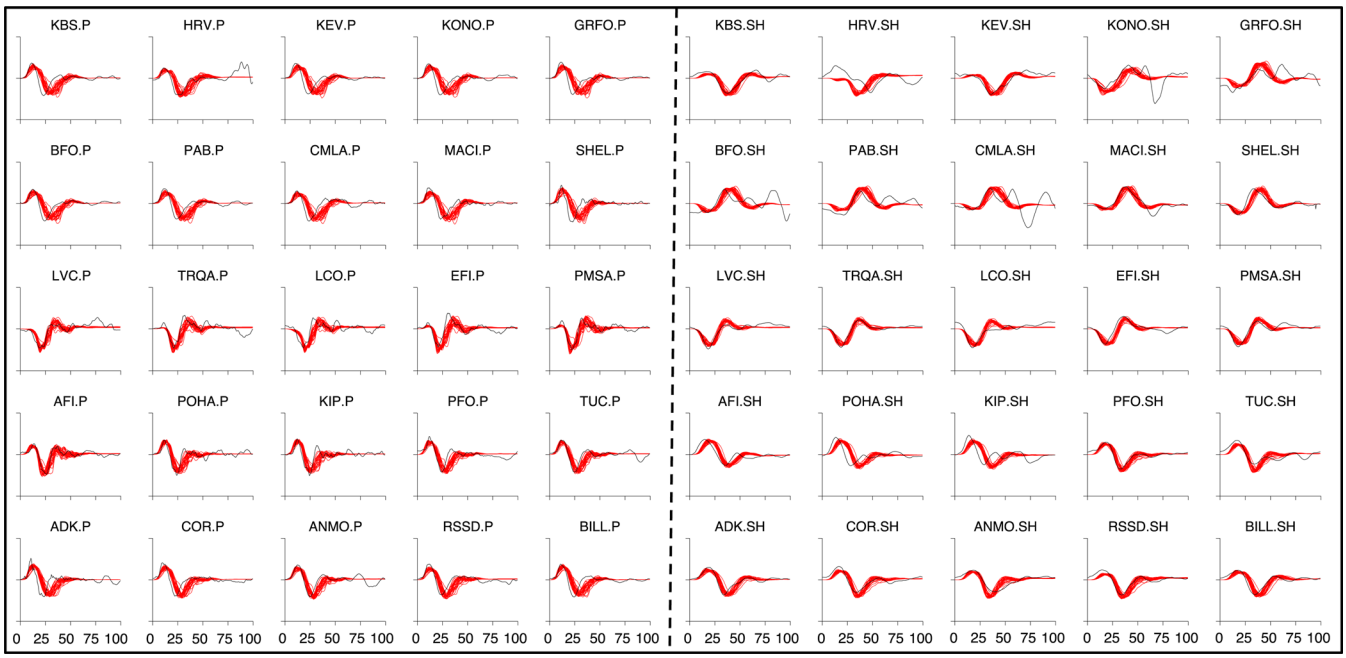

Figure 4. Waveform predictions for the first 32 random models from Fig. 1 (red seismograms) and displacement waveforms for the Nicoya earthquake (black). The significant variability of rupture patterns in Fig. 1 corresponds to relatively minor variability of synthetic waveforms, all of them providing a first order fit to the observations. Stations are sorted by azimuth from north, vertical *P* waves are shown in the left-hand panels, SH waves in the right panels.

with significantly asymmetric slip distribution but different directivity. This behaviour traces back to the dominance of the radial term in the subfault delay times (Fig. 2). Teleseismic seismograms allow for a relatively good discrimination between centred and peripherical slip patches, however the directivity detection for peripherical patches depends on the projection of the takeoff vector and translates into smaller time differences. Waveform comparison (Fig. 5) confirms that *S* waves, with smaller wave speed, are more sensitive to directivity compared to *P* waves (López-Comino *et al.* 2012). Such extreme mistakes have been hopefully prevented in published teleseismic inversions by pursuing reasonable data coverage and careful inspection of waveform fits, yet it is instructive to see the overall similarity of waveforms in this example.

THE SET OF SOLUTIONS FOR THE 2012 NICOYA EARTHQUAKE

Here we show the comparison of 10 000 model predictions to real data, how to falsify trial models, and the characteristics of the solution ensemble. We retrieve waveforms from the 2012 Nicoya earthquake through the IRIS-Wilber interface, and apply a standard pre-processing to the data. This includes cutting 1-min *P*- and *S*-wave windows, removing the instrument responses to obtain displacement waveforms, and rotating horizontal seismograms into the station backazimuth in order to isolate the SH component (Kikuchi & Kanamori 1982). Before comparison, we normalize observations and synthetics using the rms of waveform amplitudes, given that the focal mechanism and scalar seismic moment have been fixed beforehand. Normalization equalizes the weighting of observations for different wave-type, azimuth and distance, and reduces the impact of uncertainties of the fault geometry. For the application to real data, we use L1-norm misfit for seismogram comparison. L1-norm misfit is more sensitive to small amplitudes compared to other widely used distance or similarity measures such as least squares misfit or cross correlation. This is a desired property for extended fault inversion because the effects of rupture propagation mainly manifest in the duration of seismogram pulses, which for their part are usually framed by small amplitudes near the zero crossings of the traces.

First, in a brief relapse back to inversion as an inductive tool, we present the formally best fitting model (Fig. 6). It shows a simple pattern of one single slip patch, ∼70 km × ∼50 km large, with peak slip of ∼3 m close to the hypocentre. This result is similar to previous studies (Hayes 2012; Ye *et al.* 2013; Yue *et al.* 2013; Protti *et al.* 2014), validating our modelling approach. The source time function indicates a rupture duration of ∼30 s. The best model is valuable as a reference for misfit: it corresponds to overall satisfactory waveform matches. Discrepancies between data and synthetics are mainly related to near nodal *S* waves and to signal in the late part of the analysed time windows, which contains arrivals that are not addressed by the forward modelling operator. Formal normalized L1-fit is 0.4892, understanding L1-fit as unity minus normalized misfit, such that an optimal fit corresponds to a L1-fit equal one, where $u_o(t)$ and $u_s(t)$ are the observed and synthetic seismograms, respectively, considering a temporal window (t_b,t_e),

$$\mathrm{L}_1 = 1 - \left(\frac{\sum_{t_b}^{t_e} |u_o(t) - u_s(t)|}{\sum_{t_b}^{t_e} |u_o(t)|} \right). \qquad (2)$$

The waveform comparison shows that our assumptions of constant rupture velocity, rake and slip velocity function are not prejudicial to fit the observation for this earthquake. This suggests that reported rake variations (Hayes 2012; Ye *et al.* 2013; Yue *et al.* 2013; Protti *et al.* 2014) are not essential to fit teleseismic data and may belong to the null-space in this case. The same appears to hold for slip near the boundaries of the fault model, present in previous models, but nearly absent from our results due to the way we construct the trial models. Applying the principle of parsimony, we might propose to favour our model over models with more complex parametrization, however the purpose of this study is to explore uncertainties. We will now address the question whether details of

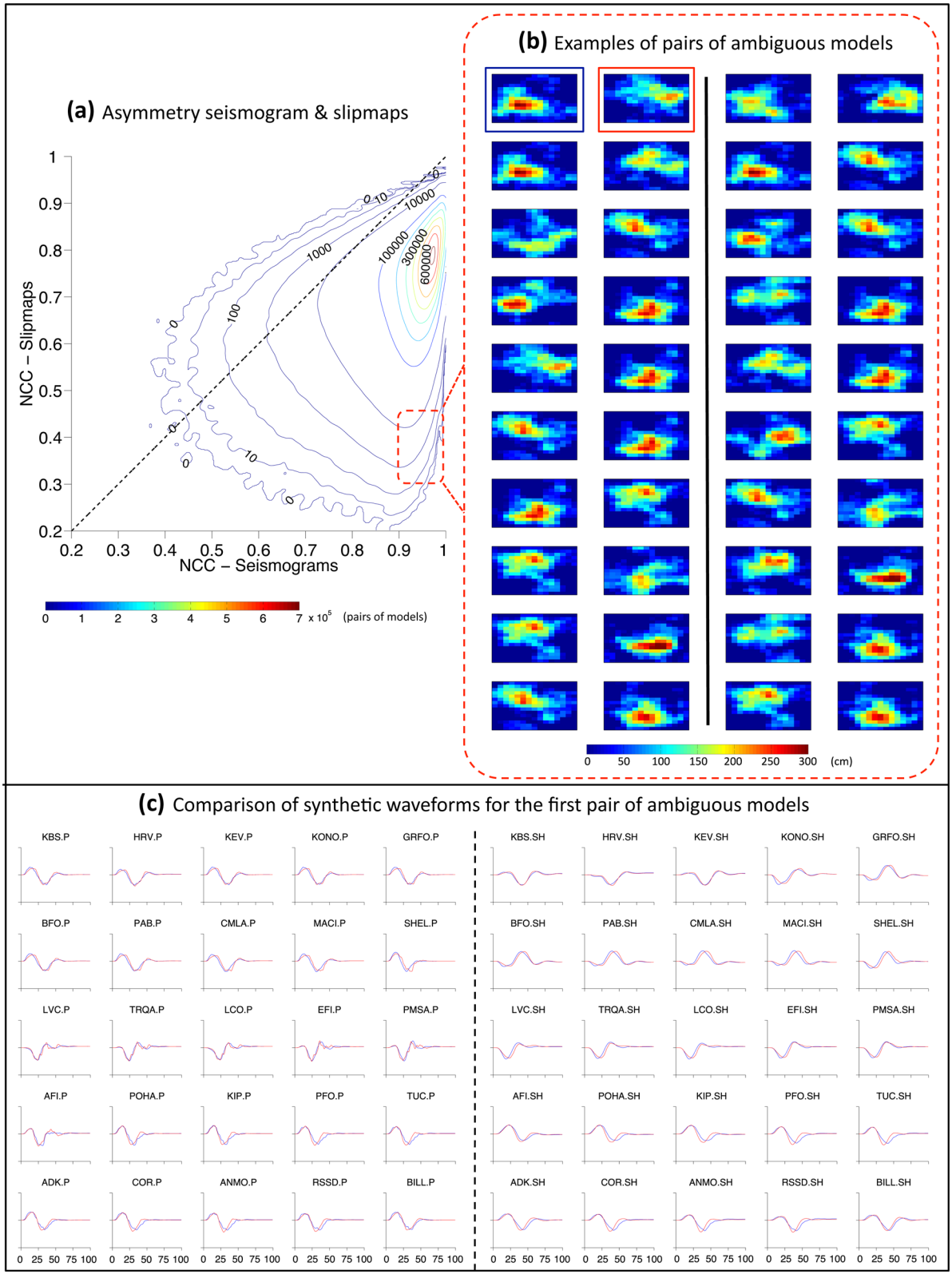

Figure 5. (a) Asymmetry between waveform similarity and slipmap similarity, displayed as contour plot for binned normalized cross-correlation (NCC) coefficients among pairs of models. Usually waveform similarity is larger than slipmap similarity, exceeding 0.9 for most pairs of models. We focus on particularly problematic pairs characterized by low slipmap correlation (<0.45) but high waveform correlation (>0.9) that may introduce ambiguity into extended fault inversion (red box). (b) Examples of slipmap pairs of ambiguous models (each row shows two pairs). All slipmaps have been normalized to the scalar moment estimate available for the Nicoya earthquake. (c) The comparison of synthetic waveforms for the first pair of ambiguous models shows that these very different slip patterns might be difficult to distinguish from recorded data (blue and red seismograms correspond to the left and right slipmaps, respectively, in the first row of Fig. 4b).

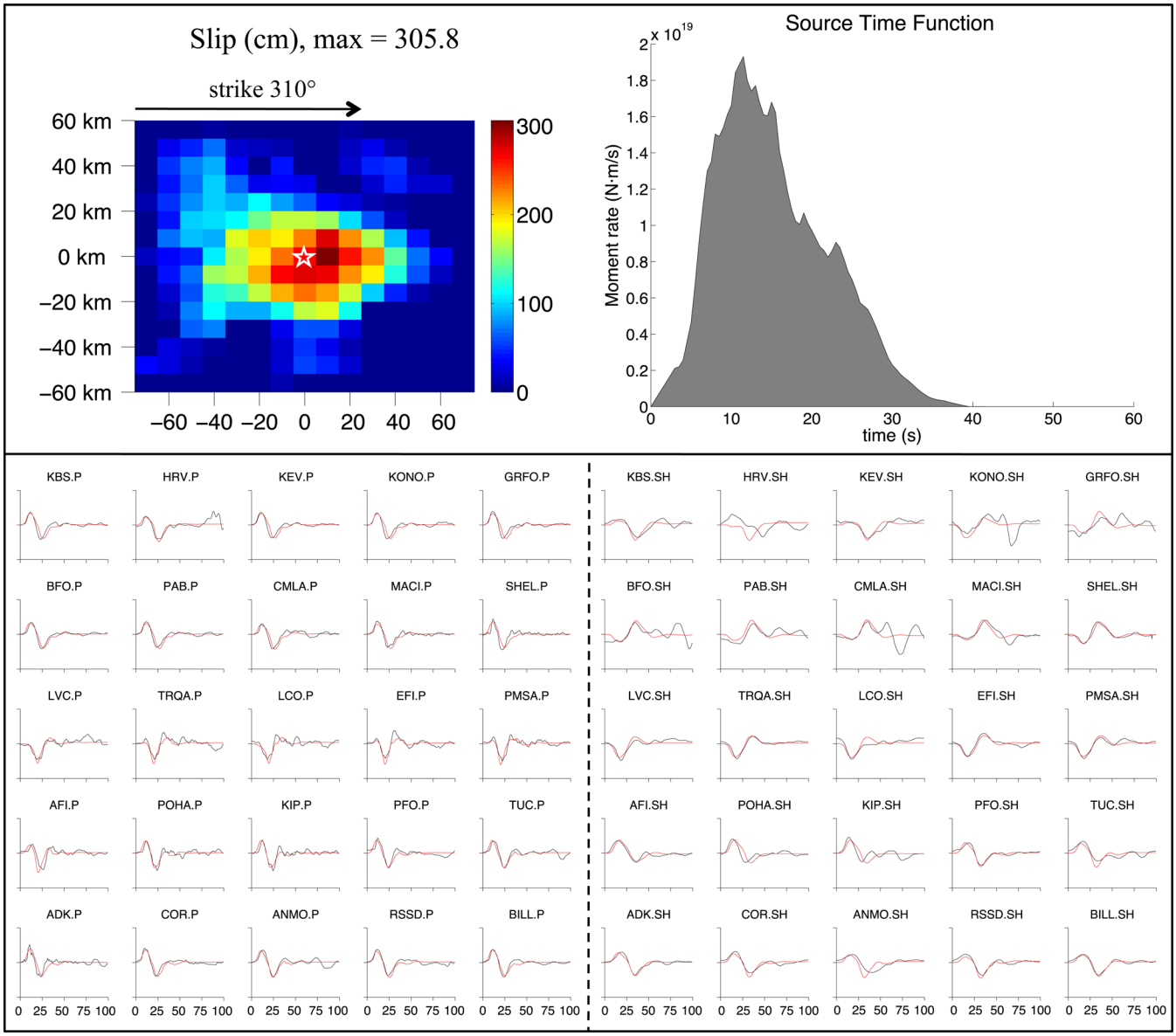

Figure 6. Best-fitting model from our inventory of random slipmaps corresponding to L1-fit of 0.4892 (upper left), associated source time function for triangular slip velocity function with 3 s half-duration on each subfault and rupture speed of 2.5 km s^{-1} (upper right), and waveform matches between predicted (red) and observed (black) displacement seismograms (stations sorted by azimuth from north).

the model such as the position of peak slip are well constrained, as well as whether a substantially different slipmap would explain the data as well.

Being based on the falsification of inappropriate slipmaps, our inversion scheme depends on criteria to decide whether a given trial model achieves an appropriate fit to the observations. For a substantial amount of models, using an objective misfit measure and threshold values automatizes this decision. We use average L1-fit to quantify similarity between seismograms. Such as any other attempt to condensate the information contained in full waveform matches into a single number, this norm is susceptible to loosing information, but we consider it a sensible choice for extended fault inversion. The introduction of a threshold value that classifies models into two categories—wrong or possibly right—is a distinctive feature of Popperian inversion. We chose the threshold based on visual inspection of waveform matches for models that achieve a given L1-norm. In our example, waveform matches with overall L1-fit of 0.4392 (5 per cent below the formally best model) are appropriate within a reasonable amount of mismodelling at most stations, while waveform matches with L1-fit of 0.3892 already show clear deficiencies compared to the best fitting model (Fig. 7; see e.g. stations KBS, KEV, GRFO, ADK and BILL for *P*-waves). The degradation of waveform matches does not affect all waveforms equally. In particular *S* waves show little variability, and also for *P* waves the differences appear at some stations and not at others. The first two station panels of Fig. 7 illustrate this behaviour. While at HRV the waveform matches are practically indistinguishable for different average L1-fit, KBS appears much more diagnostic in order to distinguish between different rupture patterns for this earthquake. The 5 per cent misfit increase already leads to a notable mismatch of *P*-wave duration compared to the best solution. On the other hand, a 10 per cent misfit increase, besides degradation of fit at individual stations, leads to a large asymmetry in normalized cross correlations between seismogram and slipmaps, showing pairs of possible

Figure 7. Comparison of waveform matches for models with different L1-fit values. In each station and wave-type (*P* or SH) panel, we show the fit of the ten best models (L1-fit between 0.4792 and 0.4892, top), 10 models with fits of L1 $\approx$ 0.4392 (best model -5 per cent, centre), and 10 models with fits of L1 $\approx$ 0.3892 (best model -10 per cent, bottom). The degradation of fits is very small for *S* waves, but fits are clearly different for *P* waves at several stations, where the formally inferior models lead to wrong predictions of *P*-wave's duration.

solutions with low similarity (Fig. 8). Then, 5 per cent misfit increase, or L1-fit of 0.4392, will be chosen as threshold for falsifying inferior trial models.

The solution set, containing 252 out of 10 000 trial models that produce L1-fit larger than 0.4392, indicates an overall satisfactory resolution of the extended fault inversion for the Nicoya earthquake (Fig. 9). All members of the solution set show a single slip patch around the hypocentre. According to a visual inspection of slipmaps, none of them is substantially different from the formally best solution, with the main slip occurring in a $\sim$70 km $\times$ $\sim$50 km large area. There is no model that suggests significant slip in other parts of the fault, or significant rupture directivity. On the other hand, the variations among acceptable models tell us what is not resolved in inversion. For example, peak slip varies between 2 and 3.5 m in the solution set (Fig. 10). Variations of almost a factor two indicate significant uncertainties for this parameter. There are

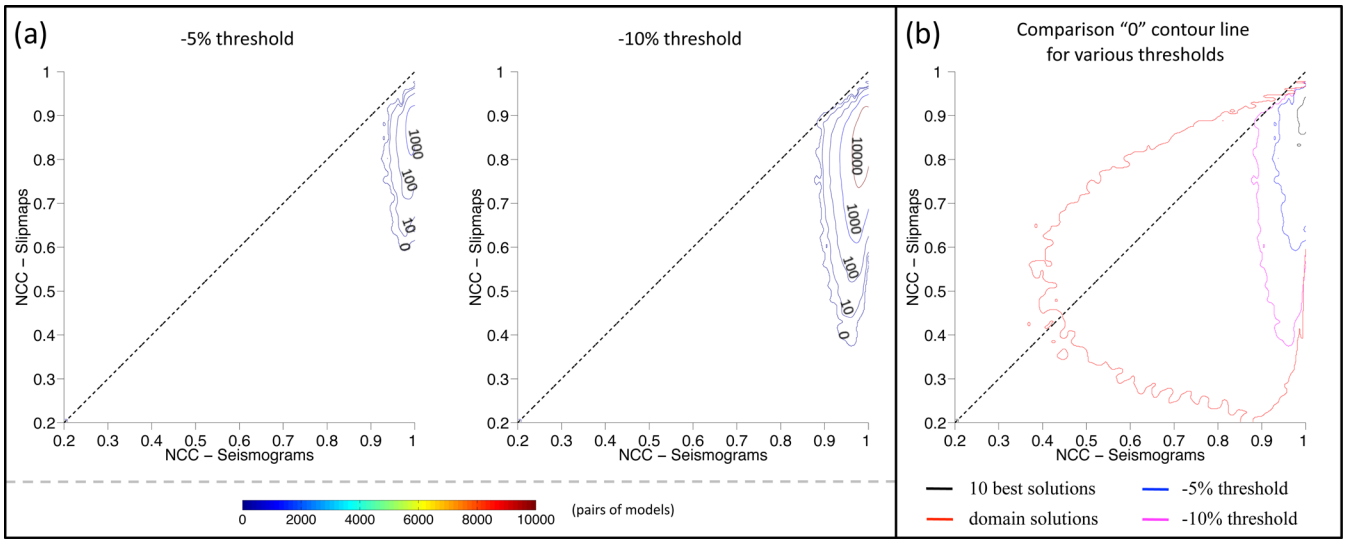

Figure 8. (a) Comparison of waveform similarity and slipmap similarity for the solution set of the Nicoya earthquake. Such as in Fig. 4(a), we display a contour plot for binned normalized cross-correlation (NCC) coefficients among pairs of possible models according to the −5 per cent threshold and −10 per cent threshold. (b) Comparison of the '0' contour lines for various thresholds: 10 formally best models, −5 per cent threshold, −10 per cent threshold as well as the entire model space (red line) for reference.

models with more concentrated slip and larger peak slip (e.g. model with L1-fit = 0.4744), compared to models with a broader slip maximum (e.g. L1 = 0.4748). In some models, peak slip splits into two relative maxima, connected by large slip close to 2 m (e.g. the second model, L1 = 0.4859). This does not suggest a description as separate patches, but it does indicate that the detailed topography of the slip patch is unresolved. This is also evident from the variability in the position of peak slip, which can be located at any direction from the hypocentre. Further uncertainties are related to the characteristics of peripheral slip in the model. While peripheral slip is *a priori* small due to the way we construct trial models, the distribution is highly variable among the solution set, suggesting that slip below 1 m may belong to the null-space. Contour plots of the slip distributions (Fig. 11) illustrate the uncertainties: The 1.5 m slip contour appears well resolved, the 2 m contour lines confining the slip maximum show significant variability, and the 1 m contour lines may extend into the periphery of the slip model. Forming the mean and the standard deviation of the solution set indicates that the most significant uncertainties occur around the 1 m contour. Source time functions (Fig. 11b) illustrate another insight for the Nicoya earthquake: The best models correspond to concentrated slip, while the misfit increases for more distributed slip that introduces delay of the moment rate maxima.

DISCUSSION

As illustrated in this study, significant differences in distributions of earthquake slip often translate into only minor variations of teleseismic body waves. In terms of the inverse problem, this implies that significant parts of the model space may correspond to similar misfit values and cannot be resolved in the presence of data and modelling uncertainties. Even in a linear setup, where we assume rupture velocity and slip velocity function to be known and only the subfault displacements have to be determined, there may exist a vast null space. Such ambiguity is well accredited for earthquake slip inversions and modellers are presumably aware of the instabilities. Nevertheless we may be sceptical of the priority given to best-fitting models produced by optimization tools (Tarantola 2006). Here we run through a Popperian inversion scheme that accounts for the asymmetry between data similarity and model similarity by falsifying inappropriate trial models and treating all remaining models as coequal solutions of the inverse problem. Assuming that the input set includes all different rupture scenarios, the solution ensemble includes all rupture models that are consistent with the observed data within some selected level of mismodelling. Different from Bayesian inversion, we do not assemble the results from model testing into a posterior probability distribution. We directly reject underperforming trial models instead of just assigning them a low degree of plausibility. Also we do not focus on the best model, although the identification of the formally best trial model is a by-product in our inversion. As in any extended fault inversion, we may expect that the best model is a rather coincidental choice among a number of possible models with similar performance. This point of view allows reducing the sampling density in the model space, making the approach inexpensive from a computational point of view. In particular, subfault Green's functions can be computed beforehand, and only the summation of subfault contributions and computation of the misfit norm needs to be repeated for each trial model.

Common with other search approaches, our extended fault inversion circumvents matrix inversion that has to be stabilized using for example subjective smoothing constraints to adjust the resolution of the model to the resolving power of the data. However, search approaches are limited by the variety of the underlying trial models, which also implicitly introducing *a priori* information into inversion. Here, the construction manual for slipmaps is derived from spectral properties of inverted fault solutions and may be affected by all their shortcomings, including nonphysical constraints applied in the original inversions. This circular logic is difficult to avoid in search schemes. Random modelling will generate fields reminiscent of earthquake slip distributions that have been seen previously, but impose limitations towards identifying any fundamentally different behaviour of the system. On the other hand, building on the body of acquired knowledge allows for keeping the model space manageable. Assuming von Karman power spectra with empirically derived correlation lengths (Mai & Beroza 2002), only a few thousand different earthquake slip distributions may be realized. Since

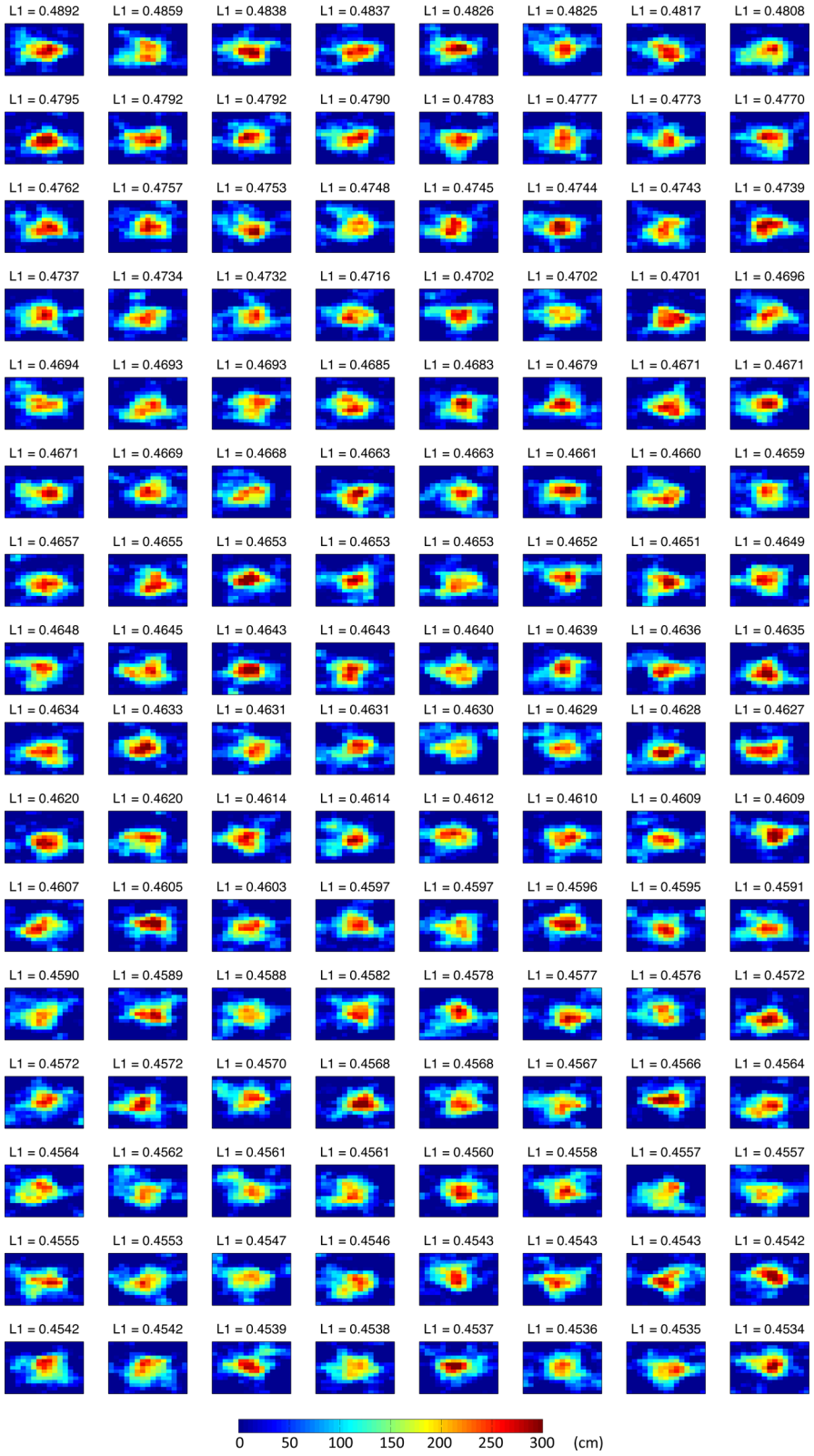

Figure 9. Solution ensemble from Popperian inversion for the Nicoya earthquake, consisting of 252 unfalsified trial models with L1-fit $\geq$ 0.4392. Slip maps are sorted according to their L1-fit (see labels), however we consider them coequal solutions of the inverse problem. Slip amplitudes are plotted using the same colour scale as in Fig. 5. Although all solutions correspond to a single dominant slip patch near the hypocentre, the variability of the solutions indicates that characteristics such as the exact position of peak slip, the concentration of slip, and the distribution of peripheral slip below 1 m are not resolved by the inversion.

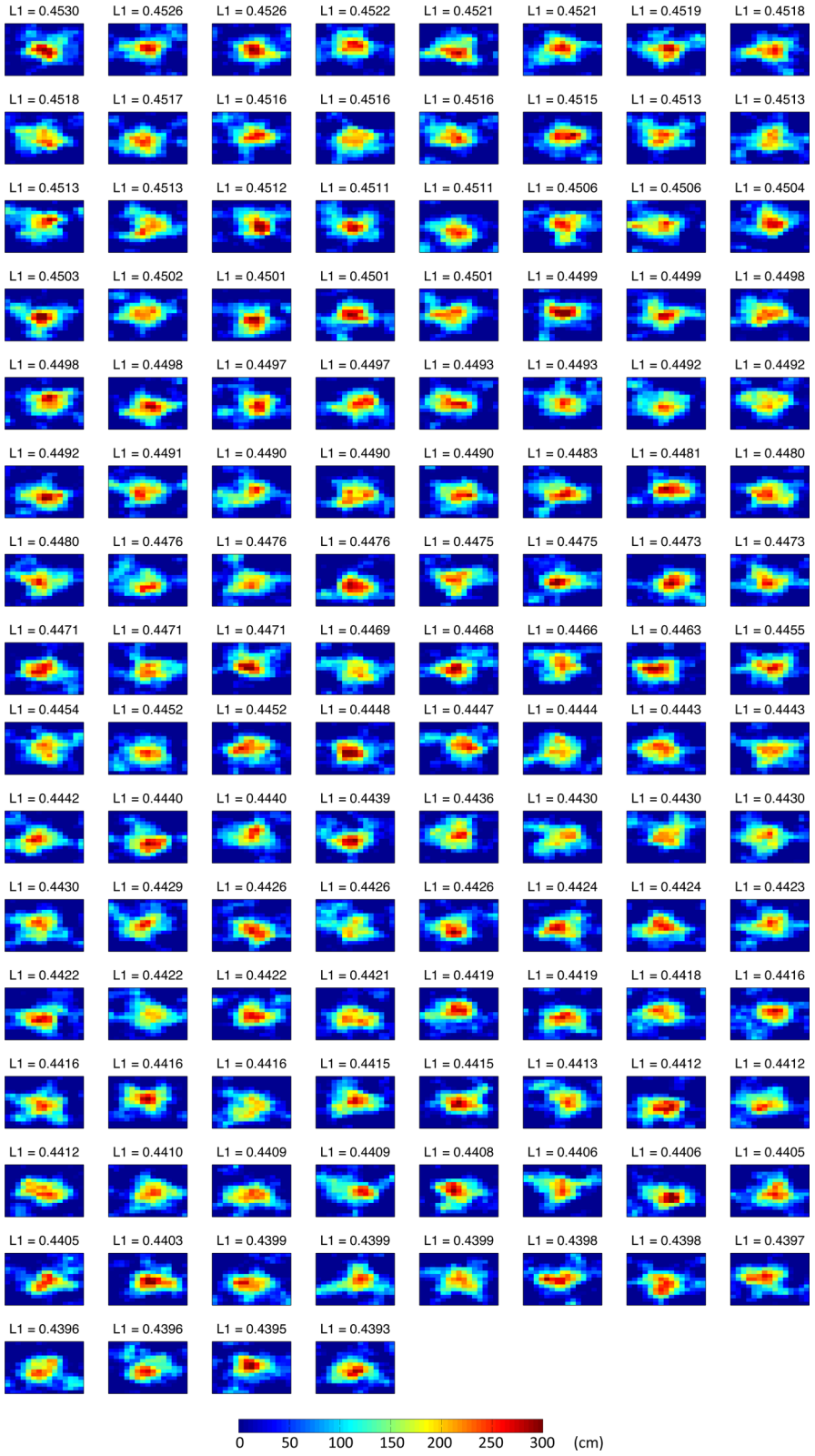

Figure 9 – *continued*

correlation length scales with fault size, at least for the resolvable part of the source model, the amount of trial models is almost independent of earthquake magnitude or fault discretization. For our example, a set of 10 000 pseudo-random maps still contains many redundancies (Fig. 1, Fig. 8) and could be condensed further. The amount of models may increase if we choose a lower Hurst number, increasing the roughness of slip. Hurst numbers around $H = 0.75$ are accredited empirically (Mai & Beroza 2002), possibly reflecting the mapping of variable rupture speed, rise time, and geometric irregularities of the fault surface onto the slip distribution. For the

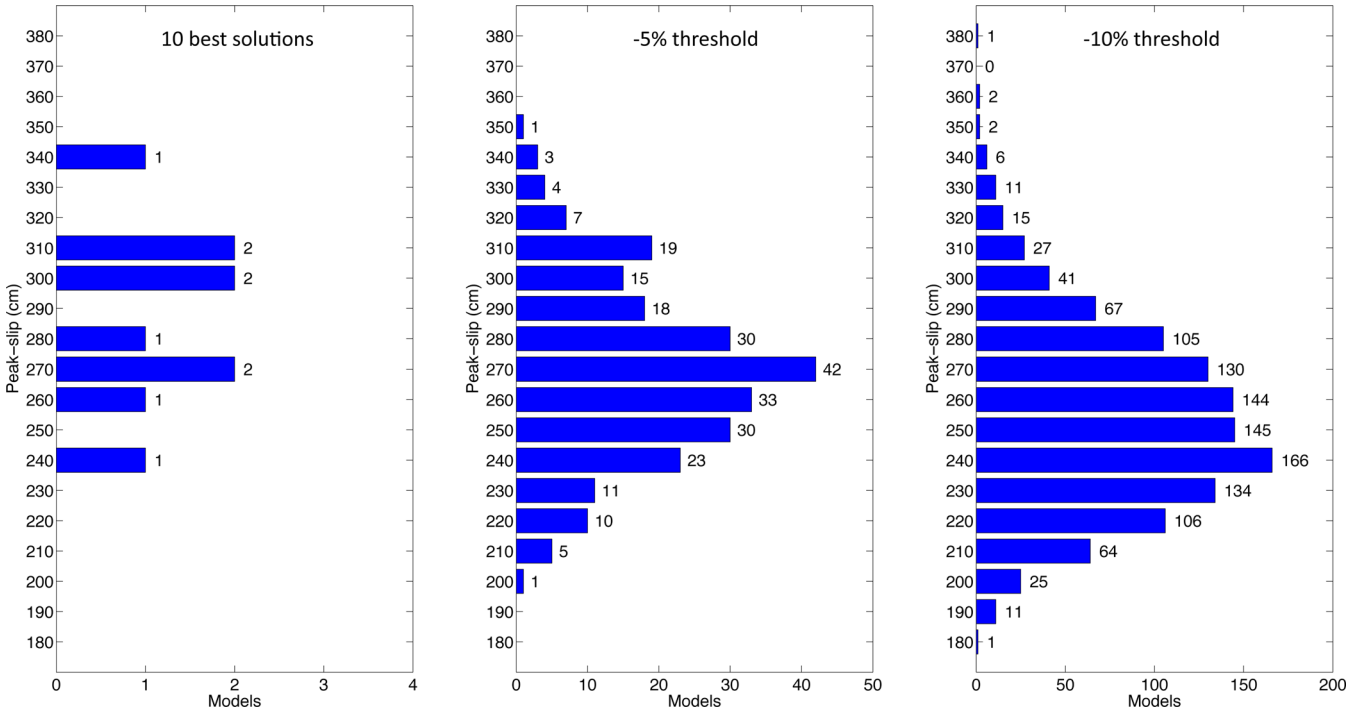

Figure 10. Comparison of peak-slip distribution for various thresholds: 10 formally best models, −5 per cent threshold and −10 per cent threshold.

data example chosen in this study, rupture models with $H = 1$ have been shown capable of fitting the observations.

Popperian inversion appears sublime from a viewpoint of philosophical aesthetics, but in practice it depends on difficult decisions about the sampling of the model space as well as misfit threshold values. As for the threshold, we have to recognize that falsification may be probabilistic in nature. There is a contradiction between the division of neighbouring models in the misfit ranking into wrong and possibly true at the chosen misfit threshold, and our expectation that the performance of these models is practically indistinguishable. In this sense, our yes-no scheme is a more primitive flavour of Bayesian approaches, and the selection of the threshold is important. A too conservative threshold causes contamination of the solution set by inferior models, while a too restrictive threshold invalidates the inversion scheme. There is probably no general-purpose solution to this dilemma, but on the positive side, Popperian inversion is well suited to incorporate meaningful misfit descriptions. Since no matrix inversion is needed, different misfit norms such as L1 and L2 can be implemented easily. Beyond that, the binary yes–no structure of Popperian inversion allows for the use of Boolean expressions. We may implement multiple thresholds for example for the misfit norm of data subsets, different misfit norms, or even for an individual observation that is considered particularly relevant. There is full flexibility in using elementary and Boolean algebra to combine different criteria and decide if a model should be considered falsified due to its overall poor performance or due to its failure in any specific aspect. In the sense of falsification, a model will be rejected through logical disjunction if it fails in one or more categories. This is particularly useful for joint inversion of different data types, for example seismic and geodetic data. The reasonable requisite of appropriate fit to each individual set of input data is straightforward to implement in Popperian logic.

To keep this proof of concept simple, we assume in this study that rupture velocity, the slip velocity function and rake values of subfault slip are known and constant across the fault. For our real data example, we obtain appropriate waveform fits under these assumptions, justifying their introduction in order to obtain a simple description for the Nicoya earthquake. More generally, there may exist trade-offs between these parameters and the slip distribution, or we may be unable to fit waveforms if the rupture is characterised by significant heterogeneity in these parameters. Actually, rake variations would not be necessary in a model scenario of a plane fault under uniform shear stress, and are sometimes suspicious to be the result of imperfect forward modelling. Variations in rupture velocity and rise time, on the other hand, are predicted by rupture dynamics. A common way to accommodate these variations is through a multiple time window scheme, where local slip histories are obtained as a superposition of time-lagged elementary functions. This introduces additional degrees of freedom, requiring substantial modification of our inversion approach in order to keep computational requirements reasonable, for example by replacing the random model generation by a guided search in the model space. Possibly a sparse parameterization of the additional model parameters that describe variable rupture speed may solve this issue, such as a search for rupture front delays only at a few key points of the slip distribution, followed by interpolation. Alternatively we may invoke earthquake dynamics; not all slip distributions are physically acceptable. Setting up the model space from dynamic rupture simulations is computationally expensive (e.g. Peyrat & Olsen 2004; Ripperger *et al.* 2008), but pseudo-dynamic slip models may represent a practicable solution. Albeit existing epistemic uncertainty, pseudo-dynamic modelling provides recipes for estimating rupture velocity and rise time from local slip amplitudes and the subfault position vector (e.g. Guatteri *et al.* 2004; Schmedes *et al.* 2010), for potential applications to complex rupture processes without relevant computational complications.

The 2012 Nicoya earthquake turns out to show a well-behaved slip distribution that can be easily reconstructed from teleseismic

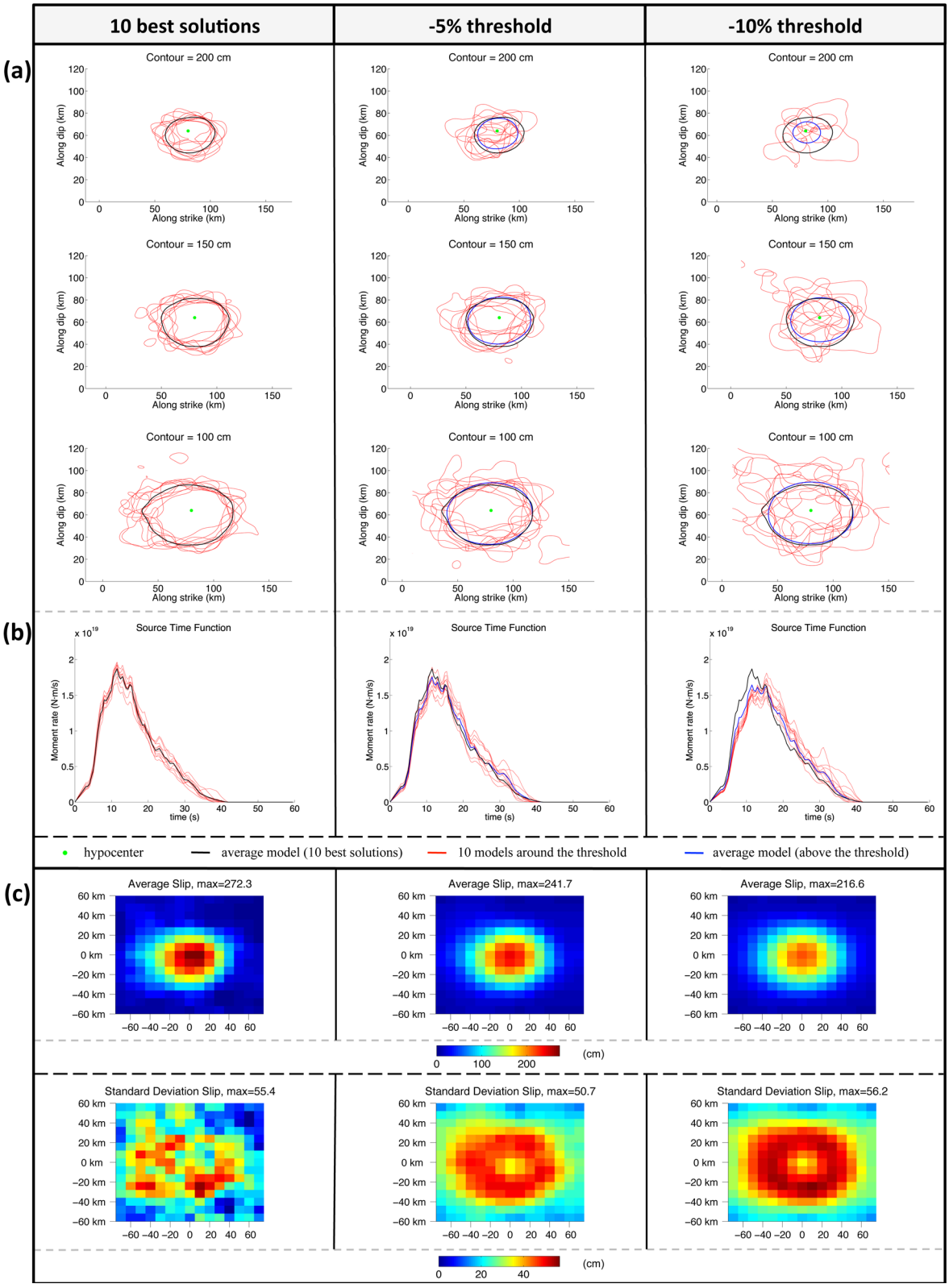

Figure 11. Comparison of properties of the 10 formally best trial models (left-hand column), models with L1-fit ≈ 0.4392 (the formally worst models included in the solution set, centre column), and models with L1-fit ≈ 0.3892 (falsified models, right-hand column). The first rows compare slip contours (2, 1.5 and 1 m) for the models, showing large scatter among falsified models, and an overall consistent behaviour for members of the solution set (black reference lines: average for the 10 formally best models, blue reference lines: average for all models above the respective threshold, red lines: 10 individual models). The same display has been chosen for the moment rate functions (4th row). Finally, the last rows show the mean and standard deviation for the 10 formally best models, all models with L1-fit ≥ 0.4392, and all models with L1-fit ≥ 0.3892, respectively.

body waves. This characteristic allows formulating a hypothesis for the source process, which may be our formally best model (Fig. 6) or any other of the 252 trial models that form the solution set and correspond to similar waveform fits. The set contains only similar solutions –a single centred slip patch- with minor differences. The similarity suggests that we could still reduce the volume of the model space, merging pairs or groups of very similar models into a single one. The minor differences between the slipmaps are interesting, because they relate to properties that are often picked out in the interpretation of fault models, such as the precise location of peak slip relative to the hypocentre. Generalizing the results for the Nicoya earthquake, viable peak slip amplitudes may have large limits of variation, and we may hardly obtain information about the total extent of rupture from finite fault inversions. Small slip in peripheric regions does not contribute significantly to the wavefield and become invisible from a practical point of view. This affects for example inferring the segmentation of major faults, confining seismic gaps, and estimating the seismic potential of plate boundaries. As an encouraging outcome, we did not undermine the legitimacy of optimization approaches in the case of the Nicoya earthquake. Proposed models (Hayes 2012; Ye *et al.* 2013; Yue *et al.* 2013; Protti *et al.* 2014) are in line with the characteristics of our solution set. In this case, previous studies certainly spent more effort on front-end issues of the inversion, such as the selection and processing of data, and Earth structure introduced into the forward operator. Popperian inversion tells us what level of detail we may venture to interpret, and warns us if inversions are not well constrained. For a solution set revealing more substantial ambiguities, a classification of slip maps according to any appropriate similarity or distance measure may help us to interpret the inversion result, propose different hypotheses for the source process, and guide the search for additional data that might possibly distinguish between the different scenarios.

ACKNOWLEDGEMENTS

We gratefully acknowledge the availability of global seismograms from the IRIS/IDA/USGS, GEOSCOPE and GEOFON networks and the IRIS DATA Centre Martin Mai kindly provided codes for generating stochastic slipmaps. We received financial support through project CGL2012-31472/BTE, Junta de Andalucia Project P09-RNM-5100 and Junta de Andalucia research group RNM 104. AMGF thanks funding by the European Commission's Initial Training Network project QUEST (contract FP7 PEOPLE-ITN-2008-238007, www.quest-itn.org) and from project AQUAREL funded by FCT (PTDC/CTE-GIX/116819/2010), Portuguese Ministry of Education and Science.

REFERENCES

Aki, K. & Richards, P.G., 2002. *Quantitative Seismology*, 2nd edn, University Science Books.

Archuleta, R.J., 1984. A faulting model for the 1979 Imperial Valley earthquake, *J. geophys. Res.,* **89,** 4559–4585.

Bean, C.J., Marsan, D. & Martini, F., 1999. Statistical measures of crustal heterogeneity from reflection seismic data: the role of seismic bandwidth, *Geophys. Res. Lett.,* **26**(21), 3241–3244.

Beresnev, I.A., 2003. Uncertainties in finite-fault slip inversions: to what extent to believe? (A critical review), *Bull. seism. Soc. Am.,* **93,** 2445–2458.

Bouchon, M., Toksöz, M.N., Karabulut, H., Bouin, M.-P., Dietrich, M., Aktar, M. & Edie, M., 2002. Space and time evolution of rupture and faulting during the 1999 İzmit (Turkey) earthquake, *Bull. seism. Soc. Am.,* **92,** 256–266.

Cohee, B.P. & Beroza, G.C., 1994. A comparison of two methods for earthquake source inversion using strong motion seismograms, *Ann. Geophys.,* **37,** 1515–1538.

Custodio, S., Liu, P.-C. & Archuleta, R.J., 2005. The 2004 M_w 6.0 Parkfield, California, earthquake: inversion of near-source ground motion using multiple data sets, *Geophys. Res. Lett.,* **32,** L23312, doi:10.1029/2005GL024417.

Delouis, B., Giardini, D., Lundgren, P. & Salichon, J., 2002. Joint inversion of InSAR, GPS, teleseismic, and strong-motion data for spatial and temporal distribution of earthquake slip: application to the 1999 Izmit Mainshock, *Bull. seism. Soc. Am.,* **92,** 278–299.

Dolan, S.S., Bean, C.J. & Riollet, B., 1998. The broad-band fractal nature of heterogeneity in the upper crust from petrophysical logs, *Geophys. J. Int.,* **132,** 489–507.

Dziewonski, A.M., Chou, T.A. & Woodhouse, J.H., 1981. Determination of earthquake source parameters from waveform data for studies of global and regional seismicity, *J. geophys. Res.,* **86**(B4), 2825–2852.

Ekström, G., Nettles, M. & Dziewonski, A.M., 2012. The global CMT project 2004–2010: centroid-moment tensors for 13 017 earthquakes, *Phys. Earth planet. Inter.,* **200–201,** 1–9.

Ferreira, A.M.G., Weston, J. & Funning, G.J., 2011. Global compilation of interferometric synthetic aperture radar earthquake source models: 2. Effects of 3-D Earth structure, *J. geophys. Res.,* **116,** B08409, doi:10.1029/2010JB008132.

Festa, G. & Zollo, A., 2012. From data to source parameters: kinematic modelling, in *The Mechanics of Faulting: From Laboratory to Real Earthquakes,* pp. 5–62, eds Bizarri, A. & Bhat, H.S., Research Signpost.

Fichtner, A. & Tkalcic, H., 2010. Insights into the kinematics of a volcanic caldera drop: probabilistic finite-source inversion of the 1996 Bardarbunga, Iceland, earthquake, *Earth planet. Sci. Lett.,* **297,** 607–615.

Fukuda, J. & Johnson, K.M., 2008. A fully bayesian inversion for spatial distribution of fault slip with objective smoothing, *Bull. seism. Soc. Am.,* **98,** 1128–1146.

Gallovič, F. & Zahradník, J., 2012. Complexity of the Mw 6.3 2009 L'Aquila (central Italy) earthquake: 1. Multiple finite-extent source inversion, *J. geophys. Res.,* **117,** B04307, doi:10.1029/2011JB008709.

Graves, R.W. & Wald, D.J., 2001. Resolution analysis of finite fault source inversion using one and three-dimensional Green's functions: 1. Strong motions, *J. geophys. Res.,* **106,** 8745–8766.

Guatteri, M., Mai, P.M. & Beroza, G.C., 2004. A pseudo-dynamic approximation to dynamic rupture models for strong ground motion pre- diction, *Bull. seism. Soc. Am.,* **94**(6), 2051–2063.

Hartzell, S.H. & Heaton, T.H., 1983. Inversion of strong ground motion and teleseismic waveform data for the fault rupture history of the 1979 Imperial Valley, California, earthquake, *Bull. seism. Soc. Am.,* **73,** 1553–1583.

Hartzell, S., Liu, P., Mendoza, C., Ji, C. & Larson, K.M., 2007. Stability and Uncertainty of Finite-Fault Slip Inversions: application to the 2004 Parkfield, California, Earthquake, *Bull. seism. Soc. Am.,* **97**(6), 1911–1934.

Hayes, G., 2012. Finite Fault Model. Preliminary Result of the Sep 5, 2012 Mw 7.6 Costa Rica Earthquake, Available at: http://earthquake.usgs.gov/earthquakes/eqinthenews/2012/usc000cfsd/finite_fault.php, last accessed 4 December 2014.

Hollinger, K., 1996. Upper-crustal seismic velocity heterogeneity as derived from a variety of *P*-wave sonic logs, *Geophys. J. Int*., **125,** 813–829.

Ide, S., Beroza, G.C. & McGuire, J.J., 2005. Imaging earthquake source complexity, in *Geophysical Monograph Series 157, Seismic Earth: Array Analysis of Broadband Seismograms,* pp. 117–135, eds Levander, A. & Nolet, G., American Geophysical Union.

Ji, C., Wald, D.J. & Helmberger, D.V., 2002. Source description of the 1999 Hector Mine, California, earthquake. Part I: wavelet domain inversion theory and resolution analysis, *Bull. seism. Soc. Am.,* **92,** 1192–1207.

Kikuchi, M. & Kanamori, H., 1982. Inversion of complex body waves, *Bull. seism. Soc. Am.,* **72,** 491–506.

Kikuchi, M. & Kanamori, H., 1991. Inversion of complex body waves III, *Bull. seism. Soc. Am.,* **81,** 2335–2350.

Kikuchi, M. & Kanamori, H., 2003. Note on teleseismic body-wave inversion program, Available at: http://geo.mff.cuni.cz/~rezba/Kiku/kikuchi's_web.html, last accessed 17 June 2015.

Lavallée, D. & Archuleta, R.J., 2003. Stochastic modeling of slip spatial complexities for the 1979 Imperial Valley, California, earthquake, *Geophys. Res. Lett.,* **30**(5), 1245.

Lavallée, D., Liu, P. & Archuleta, R.J., 2006. Stochastic model of heterogeneity in earthquake slip spatial distributions, *Geophys. J. Int.,* **165,** 622–640.

Liu, P.C., Custodio, S. & Archuleta, R.J., 2006. Kinematic inversion of the 2004 M 6.0 Parkfield earthquake including an approximation to site effects, *Bull. seism. Soc. Am.,* **96,** S143–S158.

López-Comino, J.A., Mancilla, F., Morales, J. & Stich, D., 2012. Rupture directivity of the 2011, Mw 5.2 Lorca earthquake (Spain), *Geophys. Res. Lett.,* **39,** L03301, doi:10.1029/2011GL050498.

Mai, P.M. & Beroza, G.C., 2002. A spatial random field model to characterize complexity in earthquake slip, *J. geophys. Res.,* **107**(B11), 2308, doi:10.1029/2001JB000588.

Mai, P.M., Burjanek, J., Delouis, B., Festa, G., Francois-Holden, C., Monelli, D., Uchide, T. & Zahradnik, J., 2007. Earthquake source inversion blind test: initial results and further developments, *EOS, Trans. Am. geophys. Un.,* **88**(52), Abstract S53C-08.

Minson, S.E., Simons, M. & Beck, J.L., 2013. Bayesian inversion for finite fault earthquake source models I—theory and algorithm, *Geophys. J. Int.,* **194**(3), 1701–1726.

Minson, S.E. *et al.*, 2014. Bayesian inversion for finite fault earthquake source models II: the 2011 great Tohoku-oki, Japan earthquake, *Geophys. J. Int.,* **198,** 922–940.

Monelli, D. & Mai, P.M., 2008. Bayesian inference of kinematic earthquake rupture parameters through fitting of strong motion data, *Geophys. J. Int.,* **173,** 220–232.

Olson, A.H. & Apsel, R.J., 1982. Finite faults and inverse theory with applications to the 1979 Imperial Valley earthquake, *Bull. seism. Soc. Am.,* **72,** 1969–2001.

Pardo-Igúzquiza, E. & Chica-Olmo, M., 1993. The Fourier integral method: an efficient spectral method for simulation of random fields, *Math. Geol.,* **25,** 177–217.

Peyrat, S. & Olsen, K.B., 2004. Nonlinear dynamic rupture inversion of the 2000 Western Tottori, Japan, earthquake, *Geophys. Res. Lett.,* **31,** doi:10.1029/2003GL019058.

Piatanesi, A., Cirella, A., Spudich, P. & Cocco, M., 2007. A global search inversion for earthquake kinematic rupture history: application to the 2000 western Tottori, Japan earthquake, *J. geophys. Res.,* **112,** doi:10.1029/2006JB004821.

Piatanesi, A. & Lorito, S., 2007. Rupture process of the 2004 Sumatra-Andaman earthquake from tsunami waveform inversion, *Bull. seism. Soc. Am.,* **97,** S223–S231.

Popper, K.R., 1934. *Logik der Forschung,* Akademie Verlag.

Protti, M. *et al.*, 2014. Nicoya earthquake rupture anticipated by geodetic measurement of the locked plate interface, *Nat. Geosci.,* **7,** 117–121.

Ripperger, J., Mai, P.M. & Ampuero, J.P., 2008. Variability of near-field ground-motion from dynamic earthquake rupture simulation, *Bull. seism. Soc. Am.,* **98,** 1207–1228.

Schmedes, J., Archuleta, R.J. & Lavallée, D., 2010. Correlation of earthquake source parameters inferred from dynamic rupture simulations, *J. geophys. Res.,* **115,** B03304, doi:10.1029/2009JB006689.

Sekiguchi, H. & Iwata, T., 2002. Rupture process of the 1999 Kocaeli, Turkey, earthquake estimated from strong-motion waveforms, *Bull. seism. Soc. Am.,* **92,** 300–311.

Sekiguchi, H., Irikura, K. & Iwata, T., 2000. Fault geometry at the rupture termination of the 1995 Hyogo-ken Nanbu earthquake, *Bull. seism. Soc. Am.,* **90,** 117–133.

Shao, G. & Ji, C., 2012. What the exercise of the SPICE source inversion validation BlindTest 1 did not tell you, *Geophys. J. Int.,* **189**(1), 569–590.

Stich, D., Mancilla, F. & Morales, J., 2005. Crust-mantle coupling in the Gulf of Cadiz (SW-Iberia), *Geophys. Res. Lett.,* **32,** L13306, doi:10.1029/2005GL023098.

Tarantola, A., 2006. Popper, Bayes and the inverse problem, *Nat. Phys.,* **2,** 492–494.

Tarantola, A. & Valette, B., 1982. Inverse problems = quest for information, *J. Geophys.,* **50,** 159–170.

Weston, J., Ferreira, A.M.G. & Funning, G.J., 2012. Systematic comparisons of earthquake source models determined using InSAR and seismic data, *Tectonophysics,* **532–535,** 61–81.

Weston, J., Ferreira, A.M.G. & Funning, G.J., 2014. Joint earthquake source inversions using seismo-geodesy and 3-D earth models, *Geophys. J. Int.,* **198**(2), 671–696.

Yagi, Y. & Kikuchi, M., 2000. Source rupture process of Kocaeli, Turkey, earthquake of August 17, 1999, obtained by joint inversion of near-field data and teleseismic data, *Geophys. Res. Lett.,* **27,** 1969–1972.

Ye, L., Lay, T. & Kanamori, H., 2013. Large earthquake rupture process variations on the Middle America megathrust, *Earth planet. Sci. Lett.,* **381**(0), 147–155.

Yue, H., Lay, T., Schwartz, S.Y., Rivera, L., Protti, M., Dixon, T.H., Owen, S. & Newman, A.V., 2013. The 5 September 2012 Nicoya, Costa Rica Mw 7.6 earthquake rupture process from joint inversion of high-rate GPS, strong-motion, and teleseismic *P* wave data and its relationship to adjacent plate boundary interface properties, *J. geophys. Res.,* **118,** 5453–5466.